

On the Performance of Millimeter Wave-based RF-FSO Multi-hop and Mesh Networks

Behrooz Makki*, Tommy Svensson*, *Senior Member, IEEE*, Maite Brandt-Pearce†
Senior Member, IEEE, and Mohamed-Slim Alouini‡, *Fellow, IEEE*

*Chalmers University of Technology, Gothenburg, Sweden, {behrooz.makki,
tommy.svensson}@chalmers.se

†University of Virginia, Charlottesville, VA , USA, mb-p@virginia.edu

‡ King Abdullah University of Science and Technology (KAUST), Thuwal, Saudi
Arabia, slim.alouini@kaust.edu.sa

Abstract

This paper studies the performance of multi-hop and mesh networks composed of millimeter wave (MMW)-based radio frequency (RF) and free-space optical (FSO) links. The results are obtained in cases with and without hybrid automatic repeat request (HARQ). Taking the MMW characteristics of the RF links into account, we derive closed-form expressions for the networks' outage probability and ergodic achievable rates. We also evaluate the effect of various parameters such as power amplifiers efficiency, number of antennas as well as different coherence times of the RF and the FSO links on the system performance. Finally, we determine the minimum number of the transmit antennas in the RF link such that the same rate is supported in the RF- and the FSO-based hops. The results show the efficiency of the RF-FSO setups in different conditions. Moreover, HARQ can effectively improve the outage probability/energy efficiency, and compensate for the effect of hardware impairments in RF-FSO networks. For common parameter settings of the RF-FSO dual-hop networks, outage probability of 10^{-4} and code rate of 3 nats-per-channel-use, the implementation of HARQ with a maximum of 2 and 3 retransmissions reduces the required power, compared to cases with open-loop communication, by 13 and 17 dB, respectively.

Part of this work has been accepted for presentation at the IEEE WCNC 2017.

I. INTRODUCTION

The next generation of wireless networks must provide coverage for everyone everywhere at any time. To address these demands, a combination of different techniques is considered, among which free-space optical (FSO) communication is very promising [1]–[3]. Coherent FSO systems, made inexpensive by the large fiberoptic market, provide fiber-like data rates through the atmosphere using lasers. Thus, FSO can be used for a wide range of applications such as last-mile access, fiber back-up, back-hauling and multi-hop networks. In the radio frequency (RF) domain, on the other hand, millimeter wave (MMW) communication has emerged as a key enabler to obtain sufficiently large bandwidths so that it is possible to achieve data rates comparable to those in the FSO links. In this perspective, the combination of FSO and MMW-based RF links is considered as a powerful candidate for high-rate reliable communication.

The RF-FSO related literature can be divided into two groups. The first group consists of papers on single-hop setups where the link reliability is improved via the joint implementation of RF and FSO systems. Here, either the RF and the FSO links are considered as separate links and the RF link acts as a backup when the FSO link is down, e.g., [3]–[10], or the links are combined to improve the system performance [11]–[17]. Also, the implementation of hybrid automatic repeat request (HARQ) in RF-FSO links has been considered in [17]–[19].

The second group consists of the papers analyzing the performance of multi-hop RF-FSO systems. For instance, [20], [21] study RF-FSO based relaying schemes with an RF source-relay link and an FSO or RF-FSO relay-destination link. Also, considering Rayleigh fading conditions for the RF link and amplify-and-forward relaying technique, [22], [23] derive the end-to-end error probability of the RF-FSO based setups and compare the system performance with RF-based relay networks, respectively. The impact of pointing errors on the performance of dual-hop RF-FSO systems is studied in [24]–[26]. Finally, [27] analyzes decode-and-forward techniques in multiuser relay networks using RF-FSO.

In this paper, we study the data transmission efficiency of multi-hop and mesh RF-FSO systems from an information theoretic point of view. Considering the MMW characteristics of the RF links and heterodyne detection technique in the FSO links, we derive closed-form expressions for the system outage probability (Lemmas 1-6) and ergodic achievable rates (Corollary 2). Our results are obtained for the decode-and-forward relaying approach in different cases with and without HARQ. Specifically, we show the HARQ as an effective technique to compensate for

the non-ideal properties of the RF-FSO system and improve the network reliability. We present mappings between the performance of RF- and FSO-based hops as well as between the HARQ-based and open-loop systems, in the sense that with appropriate parameter settings the same outage probability is achieved in these setups (Corollary 1, Lemma 6). Also, we determine the minimum number of transmit antennas in the RF links such that the same rate is supported by the RF- and the FSO-based hops (Corollary 2). Finally, we analyze the effect of various parameters such as the power amplifiers (PAs) efficiency, different coherence times of the RF and FSO links and number of transmit antennas on the performance of multi-hop and mesh networks.

In contrast to [1]–[19], we consider multi-hop and mesh networks. Moreover, our analytical/numerical results on the outage probability, ergodic achievable rate and the required number of antennas in HARQ-based RF-FSO systems as well as our discussions on the effect of imperfect PAs/HARQ have not been presented before. The differences in the problem formulation and the channel model makes our analytical/numerical results and conclusions completely different from the ones in the literature, e.g., [1]–[27].

The numerical and the analytical results show that:

- Depending on the codewords length, there are different methods for the analytical performance evaluation of the RF-FSO systems (Lemmas 1-6).
- There are mappings between the performance of RF- and FSO-based hops, in the sense that with proper scaling of the channel parameters the same outage probability is achieved in these hops (Corollary 1). Thus, the performance of RF-FSO based multi-hop/mesh networks can be mapped to ones using only the RF- or the FSO-based communication.
- While the network outage probability is (almost) insensitive to the number of RF-based transmit antennas when this number is large, the ergodic rate of the multi-hop network is remarkably affected by the number of antennas.
- The required number of RF-based antennas to guarantee the same rate as in the FSO-based hops increases significantly with the signal-to-noise ratio (SNR) and, at high SNRs, the ergodic rate scales with the SNR (almost) linearly.
- At low SNRs, the same outage probability is achieved in HARQ-based RF hops with N transmit antennas, a maximum of M retransmissions and C channel realizations per retransmission as with an open-loop system with MNC transmit antennas and single channel realization per codeword transmission (Lemma 6).
- The PAs efficiency affects the network outage probability/ergodic rate considerably. How-

- ever, the HARQ protocols can effectively compensate for the effect of hardware impairments.
- Finally, the HARQ improves the outage probability/energy efficiency significantly. For instance, consider common parameter settings of the RF-FSO dual-hop networks, outage probability of 10^{-4} and code rate of 3 nats-per-channel-use (npcu). Then, compared to cases with open-loop communication, the implementation of HARQ with a maximum of 2 and 3 retransmissions reduces the required power by 13 and 17 dB, respectively.

II. SYSTEM MODEL

In this section, we present the system model for a multi-hop setup with a single route from the source to the destination. As demonstrated in Section III.C, the results of the multi-hop networks can be extended to the ones in mesh networks with multiple non-overlapping routes from the source to the destination.

A. Channel Model

Consider a T^{total} -hop RF-FSO system, with T RF-based hops and $\tilde{T} = T^{\text{total}} - T$ FSO-based hops. As seen in the following, the outage probability and the ergodic achievable rate are independent of the order of the hops. Thus, we do not need to specify the order of the RF- and FSO-based hops. The i -th, $i = 1, \dots, T$, RF-based hop uses a multiple-input-single-output (MISO) setup with N_i transmit antennas. Such a setup is of interest in, e.g., side-to-side communication between buildings/lamp posts [28], as well as in wireless backhaul links where the trend is to introduce multiple antennas and thereby achieve multiple parallel streams, e.g., [29]. We define the channel gains as $g_i^{j_i} \doteq |h_i^{j_i}|^2$, $i = 1, \dots, T$, $j_i = 1, \dots, N_i$, where $h_i^{j_i}$ is the complex fading coefficients of the channel between the j_i -th antenna in the i -th hop and its corresponding receive antenna.

While the modeling of the MMW-based links is well known for line-of-sight wireless backhaul links, it is still an ongoing research topic for non-line-of-sight conditions [30]. Particularly, different measurement setups have emphasized the near-line-of-sight propagation and the non-ideal hardware as two key features of such links. Here, we present the analytical results for the quasi-static Rician channel model, with successive independent realizations, which is an appropriate model for near line-of-sight conditions and has been well established for different MMW-based applications, e.g., [31]–[33].

Let us denote the probability density function (PDF) and the cumulative distribution function (CDF) of a random variable X by $f_X(\cdot)$ and $F_X(\cdot)$, respectively. With a Rician model, the channel gain $g_i^{j_i}, \forall i, j_i$, follows the PDF

$$f_{g_i^{j_i}}(x) = \frac{(K_i + 1)e^{-K_i}}{\Omega_i} e^{-\frac{(K_i+1)x}{\Omega_i}} I_0 \left(2\sqrt{\frac{K_i(K_i + 1)x}{\Omega_i}} \right), \forall i, j_i, \quad (1)$$

where K_i and Ω_i denote the fading parameters in the i -th hop and $I_n(\cdot)$ is the n -th order modified Bessel function of the first kind. Also, defining the sum channel gain $G_i = \sum_{j_i=1}^{N_i} g_i^{j_i}$, we have

$$f_{G_i}(x) = \frac{(K_i + 1)e^{-K_i N_i}}{\Omega_i} \left(\frac{(K_i + 1)x}{K_i N_i \Omega_i} \right)^{\frac{N_i-1}{2}} e^{-\frac{(K_i+1)x}{\Omega_i}} I_{N_i-1} \left(2\sqrt{\frac{K_i(K_i + 1)N_i x}{\Omega_i}} \right), \forall i. \quad (2)$$

Finally, to take the non-ideal hardware into account, we consider the state-of-the-art model for the PA efficiency where the output power at each antenna of the i -th hop is determined according to [34, eq. (2.14)], [35, eq. (3)], [36, eq. (3)], [37, eq. (1)]

$$\frac{P_i}{P_i^{\text{cons}}} = \epsilon_i \left(\frac{P_i}{P_i^{\text{max}}} \right)_i^{\vartheta} \Rightarrow P_i = \sqrt[\vartheta]{\frac{\epsilon_i P_i^{\text{cons}}}{(P_i^{\text{max}})_i^{\vartheta}}}, \forall i. \quad (3)$$

Here, P_i, P_i^{max} and $P_i^{\text{cons}}, \forall i$, are the output, the maximum output and the consumed power in each antenna of the i -th hop, respectively, $\epsilon_i \in [0, 1]$ denotes the maximum power efficiency achieved at $P_i = P_i^{\text{max}}$ and $\vartheta_i \in [0, 1]$ is a parameter depending on the PA class.

The FSO links, on the other hand, are assumed to have single transmit/receive terminals. Reviewing the literature and depending on the channel condition, the FSO link may follow different distributions. Here, we present the results for cases with exponential and Gamma-Gamma distributions of the FSO links. For the exponential distribution of the i -th FSO hop, the channel gain \tilde{G}_i follows

$$f_{\tilde{G}_i}(x) = \lambda_i e^{-\lambda_i x}, \forall i, \quad (4)$$

with λ_i being the long-term channel coefficient of the i -th, $i = 1, \dots, \tilde{T}$, hop. Moreover, with the Gamma-Gamma distribution we have

$$f_{\tilde{G}_i}(x) = \frac{2(a_i b_i)^{\frac{a_i+b_i}{2}}}{\Gamma(a_i)\Gamma(b_i)} x^{\frac{a_i+b_i}{2}-1} \mathcal{K}_{a_i-b_i} \left(2\sqrt{a_i b_i x} \right), \forall i. \quad (5)$$

Here, $\mathcal{K}_n(\cdot)$ denotes the modified Bessel function of the second kind of order n and $\Gamma(x) = \int_0^\infty u^{x-1} e^{-u} du$ is the Gamma function. Also, a_i and $b_i, i = 1, \dots, \tilde{T}$, are the distribution shaping parameters which can be expressed as functions of the Rytov variance, e.g., [19].

B. Data Transmission Model

We consider the decode-and-forward technique where at each hop the received message is decoded and re-encoded, if it is correctly decoded. Therefore, the message is successfully received by the destination if it is correctly decoded in all hops. Otherwise, outage occurs. As the most promising HARQ approach leading to highest throughput/lowest outage probability [38]–[41], we consider the incremental redundancy (INR) HARQ with a maximum of M_i retransmissions in the i -th, $i = 1, \dots, T^{\text{total}}$, hop. Using INR HARQ with a maximum of M_i retransmissions, q_i information nats are encoded into a *parent* codeword of length $M_i L$ channel uses. The parent codeword is then divided into M_i sub-codewords of length L channel uses which are sent in the successive transmission rounds. Thus, the equivalent data rate, i.e., the code rate, at the end of round m is $\frac{q_i}{mL} = \frac{R_i}{m}$ npcu where $R_i = \frac{q_i}{L}$ denotes the initial code rate in the i -th hop. In each round, the receiver combines all received sub-codewords to decode the message. Also, different independent channel realizations may be experienced in each round of HARQ. The retransmission continues until the message is correctly decoded or the maximum permitted transmission round is reached. Note that setting $M_i = 1, \forall i$, represents the cases without HARQ, i.e., open-loop communication.

III. ANALYTICAL RESULTS

Consider the decode-and-forward approach in a multi-hop network consisting of T RF- and \tilde{T} FSO-based hops. Then, because independent channel realizations are experienced in different hops, the system outage probability is given by

$$\Pr(\text{Outage}) = 1 - \prod_{i=1}^T (1 - \phi_i) \prod_{i=1}^{\tilde{T}} (1 - \tilde{\phi}_i), \quad (6)$$

where ϕ_i and $\tilde{\phi}_i$ denote the outage probability in the i -th RF- and FSO-based hops, respectively. Note that the order of the FSO and RF links therefore do not matter. To analyze the outage probability, we need to determine ϕ_i and $\tilde{\phi}_i, \forall i$. Following the same procedure as in, e.g., [38]–[40] and using the properties of the imperfect PAs (3), the outage probability of the i -th RF- and FSO-based hops are found as

$$\phi_i = \Pr \left(\frac{1}{M_i C_i} \sum_{m=1}^{M_i} \sum_{c=(m-1)C_i+1}^{mC_i} \log \left(1 + \frac{\epsilon_i P_i^{\text{cons}}}{(P_i^{\text{max}})_i^{\vartheta}} G_i(c) \right) \leq \frac{R_i}{M_i} \right), i = 1, \dots, T, \quad (7)$$

and

$$\tilde{\phi}_i = \Pr \left(\frac{1}{M_i \tilde{C}_i} \sum_{m=1}^{M_i} \sum_{c=(m-1)\tilde{C}_i+1}^{m\tilde{C}_i} \log \left(1 + \tilde{P}_i \tilde{G}_i(c) \right) \leq \frac{R_i}{M_i} \right), i = 1, \dots, \tilde{T}, \quad (8)$$

respectively. Here, (7)-(8) come from the maximum achievable rates of Gaussian channels where, in harmony with, e.g., [12], [17], [19], [24], [25], [38], [42], we have used the Shannon's capacity formula. Thus, our results provide a lower bound of outage probability which is tight for moderate/large codewords lengths. We assume that the FSO system is well-modeled as an additive white Gaussian noise channel, with insignificant signal-dependent shot noise contribution. Moreover, \tilde{P}_i denotes the transmission power in the i -th, $i = 1, \dots, \tilde{T}$, FSO-based hop. We have considered a heterodyne detection technique in (8). Also, with no loss of generality, we have normalized the receivers' noise variances. Hence, P_i, \tilde{P}_i (in dB, $10 \log_{10} P_i, 10 \log_{10} \tilde{P}_i$) represent the SNR as well. Then, $C_i, i = 1, \dots, T$, and $\tilde{C}_i, i = 1, \dots, \tilde{T}$, represent the number of channel realizations experienced in each HARQ-based transmission round of the i -th RF- and FSO-based hops, respectively¹. The number of channel realizations experienced within a codeword transmission is determined by the channel coherence times of the links, the codewords lengths, considered frequency as well as if diversity gaining techniques such as frequency hopping are utilized. Finally, $G_i(c)$ and $\tilde{G}_i(c)$ are the sum channel gains for the channel fading realization c in the i -th RF- and FSO-based hop, respectively.

In the following, we present near-closed-form expressions for (7)-(8), and, consequently, (6). Then, Corollary 2 determines the ergodic achievable rate of multi-hop networks as well as the minimum number of required antennas in the RF-based hops to guarantee the ergodic achievable rate. Finally, Section III.C extends the results to mesh network.

Since there is no closed-form expression for the outage probabilities, we need to use different approximation techniques (see Table I for a summary of developed approximation schemes). In the first method, we concentrate on cases with long codewords where multiple channel realizations are experienced during data transmission in each hop, i.e., C_i and $\tilde{C}_i, \forall i$, are assumed to be large. Here, we use the central limit theorem (CLT) to approximate the contribution of the RF- and FSO-based hops by equivalent Gaussian random variables. Using the CLT, we find different approximation results for the network outage probability/ergodic rate (Lemmas 1-5,

¹ For simplicity, we present the results for cases with normalized symbol rates. However, using the same approach as in [12], it is straightforward to represent the results with different symbol rates of the links

Table I
SUMMARY OF DEVELOPED APPROXIMATION TECHNIQUES.

	Hop type	Metric	Tightness condition
Lemma 1	RF	Outage probability	Long codeword, low SNR
Lemmas 2-4	RF	Outage probability	Long codeword
Lemma 5	FSO	Outage probability	Long codeword
Corollary 1	RF, FSO	Outage probability	Long codeword
Corollary 2	RF, FSO	Ergodic rate/required number of antennas	Long codeword
Lemma 6	RF, FSO	Outage probability	Short codeword

Corollary 2). Then, Section III.B studies the system performance in cases with short codewords, i.e., small values of $C_i, \tilde{C}_i, \forall i$ (Lemma 6). It is important to note that the difference between the analytical schemes of Sections III.A and B comes from the values of the products $M_i C_i$ and $M_i \tilde{C}_i, \forall i$. Therefore, from (7)-(8), the long-codeword results of Section III.A can be also mapped to cases with short codewords, large number of retransmissions and scaled code rates. As shown in Section IV, our derived analytical results are in high agreement with the numerical simulations.

A. Performance Analysis with Long Codewords

Lemma 1: At low SNRs, the outage probability (7) is approximately given by (15) with μ_i and σ_i^2 defined in (10) and (11), respectively.

Proof. Using $\log(1+x) \simeq x$ for small values of x , (7) is rephrased as

$$\phi_i \simeq \Pr \left(\frac{1}{M_i C_i} \sum_{m=1}^{M_i} \sum_{c=(m-1)C_i+1}^{mC_i} G_i(c) \leq \frac{R_i}{M_i^{1-\vartheta_i} \sqrt{\frac{\epsilon_i P_i^{\text{cons}}}{(P_i^{\text{max}})^{\vartheta_i}}}} \right), \quad (9)$$

where for long codewords/large number of retransmissions, we can use the CLT to replace the random variable $\frac{1}{M_i C_i} \sum_{m=1}^{M_i} \sum_{c=(m-1)C_i+1}^{mC_i} G_i(c)$ by an equivalent Gaussian variable $\mathcal{V}_i \sim \mathcal{N}(\mu_i, \frac{1}{M_i C_i} \sigma_i^2)$ with

$$\mu_i = \int_0^\infty x f_{G_i}(x) \stackrel{(a)}{=} \frac{\Omega_i e^{-K_i N_i} N_i}{K_i + 1} {}_1F_1(N_i + 1; N_i; K_i N_i), \quad (10)$$

and

$$\begin{aligned} \sigma_i^2 &= \gamma_i - \mu_i^2, \\ \gamma_i &= \int_0^\infty x^2 f_{G_i}(x) \stackrel{(b)}{=} \frac{\Omega_i^2 e^{-K_i N_i (N_i + 1)} N_i}{(K_i + 1)^2} {}_1F_1(N_i + 2; N_i; K_i N_i). \end{aligned} \quad (11)$$

Here, ${}_sF_t(a_1, \dots, a_s; b_1, \dots, b_t; x) = \sum_{j=0}^{\infty} \frac{(a_1)_j \dots (a_s)_j}{(b_1)_j \dots (b_t)_j} \left(\frac{x^j}{j!}\right)$, $(a)_0 = 1$, $(a)_j = a(a+1) \dots (a+j-1)$, $j > 0$, denotes the generalized hypergeometric function. Also, to find (a)-(b) we have first used the property [43, eq. (03.02.26.0002.01)]

$$I_n(x) = \frac{1}{\Gamma(n+1)} \left(\frac{x}{2}\right)^n {}_0F_1\left(n+1; \frac{x^2}{4}\right), \quad (12)$$

to represent the PDF (2) as

$$f_{G_i}(x) = \frac{(K_i+1)^{N_i} e^{-K_i N_i}}{\Omega_i^{N_i} \Gamma(N_i)} x^{N_i-1} e^{-\frac{(K_i+1)x}{\Omega_i}} {}_0F_1\left(N_i; \frac{K_i(K_i+1)N_i x}{\Omega_i}\right), \quad (13)$$

and then derived (a)-(b) based on the following integral identity [44, eq. (7.522.5)]

$$\begin{aligned} & \int_0^{\infty} e^{-x} x^{\nu-1} {}_sF_t(a_1, \dots, a_s; b_1, \dots, b_t; \alpha x) dx \\ &= \Gamma(\nu) {}_{s+1}F_t(\nu, a_1, \dots, a_s; b_1, \dots, b_t; \alpha). \end{aligned} \quad (14)$$

In this way, using the CDF of Gaussian random variables and the error function $\text{erf}(x) = \frac{2}{\sqrt{\pi}} \int_0^x e^{-t^2} dt$, (7) is obtained by

$$\phi_i \simeq \Pr\left(\mathcal{V}_i \leq \frac{R_i}{M_i^{1-\vartheta_i} \sqrt{\frac{\epsilon_i P_i^{\text{cons}}}{(P_i^{\text{max}})^{\vartheta_i}}}}\right) = \frac{1}{2} \left(1 + \text{erf}\left(\frac{\sqrt{M_i C_i} \left(\frac{R_i}{M_i^{1-\vartheta_i} \sqrt{\frac{\epsilon_i P_i^{\text{cons}}}{(P_i^{\text{max}})^{\vartheta_i}}}} - \mu_i\right)}{\sqrt{2\sigma_i^2}}\right)\right), \quad (15)$$

as stated in the lemma. \square

To present the second approximation method for (7), we first represent an approximate expression for the PDF of the sum channel gain $G_i, \forall i$, as follows.

Lemma 2: For moderate/large number of antennas, which is of interest in MMW communication, the sum gain $G_i, \forall i$, is approximated by an equivalent Gaussian random variable $\mathcal{Z}_i \sim \mathcal{N}(N_i \zeta_i, N_i \nu_i^2)$ with $\zeta_i = \mathcal{S}_i(2)$, $\nu_i^2 = \mathcal{S}_i(4) - \mathcal{S}_i(2)^2$ and $\mathcal{S}_i(n) \doteq \left(\frac{\Omega_i}{K_i+1}\right)^{\frac{n}{2}} \Gamma\left(1 + \frac{n}{2}\right) \mathcal{L}_{\frac{n}{2}}(-K_i)$. Here, $\mathcal{L}_n(x) = \frac{e^{-x}}{n!} \frac{d^n}{dx^n} (e^{-x} x^n)$ denotes the Laguerre polynomial of the n -th order and K_i, Ω_i are the fading parameters as defined in (1).

Proof. Using the CLT for moderate/large number of antennas, the random variable $G_i = \sum_{j_i=1}^{N_i} g_i^{j_i}$ is approximated by the Gaussian random variable $\mathcal{Z}_i \sim \mathcal{N}(N_i \zeta_i, N_i \nu_i^2)$. Here, from (1), ζ_i and ν_i^2 are, respectively, determined by

$$\zeta_i = \int_0^{\infty} x f_{g_i^{j_i}}(x) dx = \frac{(K_i+1)e^{-K_i}}{\Omega_i} \int_0^{\infty} x e^{-\frac{(K_i+1)x}{\Omega_i}} I_0\left(2\sqrt{\frac{K_i(K_i+1)x}{\Omega_i}}\right) dx, \quad (16)$$

and

$$\nu_i^2 = \rho_i - \zeta_i^2,$$

$$\rho_i = \int_0^\infty x^2 f_{g_i^{j_i}}(x) dx = \frac{(K_i + 1)e^{-K_i}}{\Omega_i} \int_0^\infty x^2 e^{-\frac{(K_i+1)x}{\Omega_i}} I_0 \left(2\sqrt{\frac{K_i(K_i+1)x}{\Omega_i}} \right) dx, \quad (17)$$

which, using the variable transform $t = \sqrt{x}$, some manipulations and the properties of the Bessel function $\frac{1}{b^2} \int_0^\infty x^{n+1} e^{-\frac{x^2+c^2}{2b^2}} I_0 \left(\frac{cx}{b^2} \right) dx = b^n 2^{\frac{n}{2}} \Gamma \left(1 + \frac{n}{2} \right) \mathcal{L} \left(\frac{-c^2}{2b^2} \right)$, $\forall c, b, n$, are determined as stated in the lemma. \square

Lemma 3: The outage probability (7) is approximated by (22) with $\hat{\mu}_i$ and $\hat{\sigma}_i^2$ given in (19)-(20), respectively.

Proof. Replacing the random variable $\frac{1}{M_i C_i} \sum_{m=1}^{M_i} \sum_{c=(m-1)C_i+1}^{mC_i} \log \left(1 + \sqrt[1-\vartheta_i]{\frac{\epsilon_i P_i^{\text{cons}}}{(P_i^{\text{max}})_i^{\vartheta_i}} G_i(c)} \right)$ by its equivalent Gaussian random variable $\mathcal{U}_i \sim \mathcal{N} \left(\hat{\mu}_i, \frac{1}{M_i C_i} \hat{\sigma}_i^2 \right)$, the probability (7) is rephrased as

$$\phi_i \simeq \Pr \left(\mathcal{U}_i \leq \frac{R_i}{M_i} \right), \mathcal{U}_i \sim \mathcal{N} \left(\hat{\mu}_i, \frac{1}{M_i C_i} \hat{\sigma}_i^2 \right), \quad (18)$$

where

$$\begin{aligned} \hat{\mu}_i &= \int_0^\infty \log \left(1 + \sqrt[1-\vartheta_i]{\frac{\epsilon_i P_i^{\text{cons}}}{(P_i^{\text{max}})_i^{\vartheta_i}} x} \right) f_{G_i}(x) dx \stackrel{(c)}{\simeq} \int_0^\infty \mathcal{Y}_i(x) f_{\mathcal{Z}_i}(x) dx \\ &= \mathcal{Q} \left(\sqrt[1-\vartheta_i]{\frac{\epsilon_i P_i^{\text{cons}}}{(P_i^{\text{max}})_i^{\vartheta_i}}}, 0, N_i \zeta_i, N_i \nu_i^2, s_i \right) - \mathcal{Q} \left(\sqrt[1-\vartheta_i]{\frac{\epsilon_i P_i^{\text{cons}}}{(P_i^{\text{max}})_i^{\vartheta_i}}}, 0, N_i \zeta_i, N_i \nu_i^2, 0 \right) \\ &\quad + \mathcal{Q} \left(r_i, \theta - r_i d_i, N_i \zeta_i, N_i \nu_i^2, \infty \right) - \mathcal{Q} \left(r_i, \theta - r_i d_i, N_i \zeta_i, N_i \nu_i^2, s_i \right), \\ \mathcal{Q}(a_1, a_2, a_3, a_4, x) &\doteq -\frac{a_1 a_3 + a_2}{2} \text{erf} \left(\frac{a_3 - x}{\sqrt{2a_4}} \right) - \frac{a_4}{2\pi} a_1 e^{-\frac{(a_3 - x)^2}{2a_4}}, \end{aligned} \quad (19)$$

and

$$\begin{aligned}
\hat{\sigma}_i^2 &= \hat{\gamma}_i - \hat{\mu}_i^2, \\
\hat{\gamma}_i &= \int_0^\infty \log^2 \left(1 + \sqrt[1-\vartheta_i]{\frac{\epsilon_i P_i^{\text{cons}}}{(P_i^{\text{max}})_i} x} \right) f_{G_i}(x) dx \stackrel{(d)}{\simeq} \int_0^\infty \mathcal{Y}_i^2(x) f_{Z_i}(x) dx \\
&= \mathcal{T} \left(\sqrt[1-\vartheta_i]{\frac{\epsilon_i P_i^{\text{cons}}}{(P_i^{\text{max}})_i}}, 0, N_i \zeta_i, N_i \nu_i^2, s_i \right) - \mathcal{T} \left(\sqrt[1-\vartheta_i]{\frac{\epsilon_i P_i^{\text{cons}}}{(P_i^{\text{max}})_i}}, 0, N_i \zeta_i, N_i \nu_i^2, 0 \right) \\
&\quad + \mathcal{T} \left(r_i, \theta - r_i d_i, N_i \zeta_i, N_i \nu_i^2, \infty \right) - \mathcal{T} \left(r_i, \theta - r_i d_i, N_i \zeta_i, N_i \nu_i^2, s_i \right), \\
\mathcal{T} \left(a_1, a_2, a_3, a_4, x \right) &\doteq \frac{1}{2\sqrt{2\pi}} e^{-\frac{x^2+a_3^2}{2a_4}} \left(\text{erf} \left(\frac{x-a_3}{\sqrt{2a_4}} \right) - 2\sqrt{a_4} a_1 e^{\frac{a_3 x}{a_4}} (a_1(a_3+x) + 2a_2) \right. \\
&\quad \left. + \sqrt{2\pi} e^{\frac{x^2+a_3^2}{2a_4}} (a_1^2(a_3^2+a_4) + 2a_1 a_2 a_3 + a_2^2) \right). \tag{20}
\end{aligned}$$

Here, (c) and (d) in (19) and (20) come from approximating $f_{G_i}(x)$ by $f_{Z_i}(x)$ defined in Lemma 2 and the approximation $\log \left(1 + \sqrt[1-\vartheta_i]{\frac{\epsilon_i P_i^{\text{cons}}}{(P_i^{\text{max}})_i} x} \right) \simeq \mathcal{Y}_i(x)$ where

$$\begin{aligned}
\mathcal{Y}_i(x) &= \begin{cases} \sqrt[1-\vartheta_i]{\frac{\epsilon_i P_i^{\text{cons}}}{(P_i^{\text{max}})_i} x}, & x \in [0, s_i] \\ \theta + r_i(x - d_i), & x > s_i, \end{cases}, \\
s_i &= \frac{\theta}{\sqrt[1-\vartheta_i]{\frac{\epsilon_i P_i^{\text{cons}}}{(P_i^{\text{max}})_i} (1 - e^{-\theta})}} - \frac{1}{\sqrt[1-\vartheta_i]{\frac{\epsilon_i P_i^{\text{cons}}}{(P_i^{\text{max}})_i}}}, \\
r_i &= \sqrt[1-\vartheta_i]{\frac{\epsilon_i P_i^{\text{cons}}}{(P_i^{\text{max}})_i}} e^{-\theta}, \quad d_i = \frac{e^\theta - 1}{\sqrt[1-\vartheta_i]{\frac{\epsilon_i P_i^{\text{cons}}}{(P_i^{\text{max}})_i}}}. \tag{21}
\end{aligned}$$

Then, following the same procedure as in (15), (18) is obtained as

$$\phi_i \simeq \frac{1}{2} \left(1 + \text{erf} \left(\frac{\sqrt{M_i C_i} \left(\frac{R_i}{M_i} - \hat{\mu}_i \right)}{\sqrt{2\hat{\sigma}_i^2}} \right) \right), \quad \forall \theta > 0. \tag{22}$$

Note that, in (19)-(22), $\theta > 0$ is an arbitrary parameter and, based on our simulations, accurate approximations are obtained for a broad range of $\theta > 0$. \square

Lemma 4: The outage probability of the RF-hop, i.e., (7), is approximately given by

$$\phi_i \simeq \frac{1}{2} \left(1 + \text{erf} \left(\frac{\sqrt{M_i C_i} \left(\frac{R_i}{M_i} - \check{\mu}_i \right)}{\sqrt{2\check{\sigma}_i^2}} \right) \right), \tag{23}$$

with $\check{\mu}_i$ and $\check{\sigma}_i^2$ defined in (24) and (26), respectively.

Proof. To prove the lemma, we again use the CLT where the achievable rate random variable

$$\begin{aligned}
& \frac{1}{M_i C_i} \sum_{m=1}^{M_i} \sum_{c=(m-1)C_i+1}^{mC_i} \log \left(1 + {}^{1-\vartheta_i} \sqrt{\frac{\epsilon_i P_i^{\text{cons}}}{(P_i^{\text{max}})_i}} G_i(c) \right) \text{ is replaced by } \check{\mathcal{U}}_i \sim \mathcal{N}(\check{\mu}_i, \frac{1}{M_i C_i} \check{\sigma}_i^2) \text{ with} \\
\check{\mu}_i &= \int_0^\infty \log \left(1 + {}^{1-\vartheta_i} \sqrt{\frac{\epsilon_i P_i^{\text{cons}}}{(P_i^{\text{max}})_i}} x \right) f_{G_i}(x) dx \stackrel{(e)}{\simeq} {}^{1-\vartheta_i} \sqrt{\frac{\epsilon_i P_i^{\text{cons}}}{(P_i^{\text{max}})_i}} \int_0^\infty \frac{1 - F_{Z_i}(x)}{1 + {}^{1-\vartheta_i} \sqrt{\frac{\epsilon_i P_i^{\text{cons}}}{(P_i^{\text{max}})_i}} x} dx \\
& \stackrel{(f)}{\simeq} {}^{1-\vartheta_i} \sqrt{\frac{\epsilon_i P_i^{\text{cons}}}{(P_i^{\text{max}})_i}} \int_0^\infty \frac{\mathcal{W}_i(x)}{1 + {}^{1-\vartheta_i} \sqrt{\frac{\epsilon_i P_i^{\text{cons}}}{(P_i^{\text{max}})_i}} x} dx = \log \left(1 + {}^{1-\vartheta_i} \sqrt{\frac{\epsilon_i P_i^{\text{cons}}}{(P_i^{\text{max}})_i}} \left(\frac{-\sqrt{2\pi N_i \nu_i^2}}{2} + N_i \zeta_i \right) \right) \\
& + \mathcal{A}_i \left({}^{1-\vartheta_i} \sqrt{\frac{\epsilon_i P_i^{\text{cons}}}{(P_i^{\text{max}})_i}}, \frac{-1}{\sqrt{2\pi N_i \nu_i^2}}, \frac{1}{2} + \frac{N_i \zeta_i}{\sqrt{2\pi N_i \nu_i^2}}, \frac{-\sqrt{2\pi N_i \nu_i^2}}{2} + N_i \zeta_i \right) \\
& - \mathcal{A}_i \left({}^{1-\vartheta_i} \sqrt{\frac{\epsilon_i P_i^{\text{cons}}}{(P_i^{\text{max}})_i}}, \frac{-1}{\sqrt{2\pi N_i \nu_i^2}}, \frac{1}{2} + \frac{N_i \zeta_i}{\sqrt{2\pi N_i \nu_i^2}}, \frac{\sqrt{2\pi N_i \nu_i^2}}{2} + N_i \zeta_i \right), \\
\mathcal{A}(a_1, a_2, a_3, x) & \doteq \frac{a_1 a_2 x^2}{2} \log(1 + a_1 x) - \frac{a_1 a_2 x^2}{4} - \frac{a_2 \log(1 + a_1 x)}{2a_1} - a_1 a_3 x + a_1 a_3 x \log(1 + a_1 x) \\
& + a_3 \log(1 + a_1 x) + \frac{a_2 x}{2}. \tag{24}
\end{aligned}$$

Here, (e) comes from Lemma 2 and partial integration. Then, (f) is obtained by the linearization technique $Q \left(\frac{x - N_i \zeta_i}{\sqrt{N_i \nu_i^2}} \right) \simeq \mathcal{W}_i(x)$ with

$$\mathcal{W}_i(x) \doteq \begin{cases} 1 & \text{if } x \leq \frac{-\sqrt{2\pi N_i \nu_i^2}}{2} + N_i \zeta_i, \\ \frac{1}{2} - \frac{1}{\sqrt{2\pi N_i \nu_i^2}} (x - N_i \zeta_i) & \text{if } x \in \left[\frac{-\sqrt{2\pi N_i \nu_i^2}}{2} + N_i \zeta_i, \frac{\sqrt{2\pi N_i \nu_i^2}}{2} + N_i \zeta_i \right], \\ 0 & \text{if } x > \frac{\sqrt{2\pi N_i \nu_i^2}}{2} + N_i \zeta_i, \end{cases} \tag{25}$$

which is found by linearly approximating $Q \left(\frac{x - N_i \zeta_i}{\sqrt{N_i \nu_i^2}} \right)$ near the point $x = N_i \zeta_i$. Finally, the last equality is obtained by partial integration and some manipulations. Also, following the same

procedure, we have

$$\check{\sigma}_i^2 = \check{\rho}_i - \check{\mu}_i^2$$

$$\begin{aligned} \check{\rho} &= \int_0^\infty \log^2 \left(1 + \sqrt[1-\vartheta_i]{\frac{\epsilon_i P_i^{\text{cons}}}{(P_i^{\text{max}})_i} x} \right) f_{G_i}(x) dx \simeq 2 \sqrt[1-\vartheta_i]{\frac{\epsilon_i P_i^{\text{cons}}}{(P_i^{\text{max}})_i}} \int_0^\infty \frac{\log \left(1 + \sqrt[1-\vartheta_i]{\frac{\epsilon_i P_i^{\text{cons}}}{(P_i^{\text{max}})_i} x} \right) \mathcal{W}_i(x)}{1 + \sqrt[1-\vartheta_i]{\frac{\epsilon_i P_i^{\text{cons}}}{(P_i^{\text{max}})_i} x}} dx \\ &= \log^2 \left(1 + \sqrt[1-\vartheta_i]{\frac{\epsilon_i P_i^{\text{cons}}}{(P_i^{\text{max}})_i}} \left(\frac{-\sqrt{2\pi N_i \nu_i^2}}{2} + N_i \zeta_i \right) \right) \\ &+ \mathcal{B}_i \left(\sqrt[1-\vartheta_i]{\frac{\epsilon_i P_i^{\text{cons}}}{(P_i^{\text{max}})_i}}, \frac{-1}{\sqrt{2\pi N_i \nu_i^2}}, \frac{1}{2} + \frac{N_i \zeta_i}{\sqrt{2\pi N_i \nu_i^2}}, \frac{-\sqrt{2\pi N_i \nu_i^2}}{2} + N_i \zeta_i \right) \\ &- \mathcal{B}_i \left(\sqrt[1-\vartheta_i]{\frac{\epsilon_i P_i^{\text{cons}}}{(P_i^{\text{max}})_i}}, \frac{-1}{\sqrt{2\pi N_i \nu_i^2}}, \frac{1}{2} + \frac{N_i \zeta_i}{\sqrt{2\pi N_i \nu_i^2}}, \frac{\sqrt{2\pi N_i \nu_i^2}}{2} + N_i \zeta_i \right), \\ \mathcal{B}(a_1, a_2, a_3, x) &\doteq \frac{a_1 a_3 - a_2}{a_1} \log^2(1 + a_1 x) - 2a_2 x + \frac{2a_1 a_2 x + 2a_2}{a_1} \log(1 + a_1 x). \end{aligned} \quad (26)$$

In this way, the outage probability is given by (23). \square

Finally, Lemma 5 represents the outage probability of the FSO-based hops as follows.

Lemma 5: The outage probability of the FSO-based hop, i.e., (8), is approximately given by

$$\tilde{\phi}_i \simeq \frac{1}{2} \left(1 + \operatorname{erf} \left(\frac{\sqrt{M_i \tilde{C}_i} \left(\frac{R_i}{M_i} - \tilde{\mu}_i \right)}{\sqrt{2\tilde{\sigma}_i^2}} \right) \right), \quad (27)$$

where $\tilde{\mu}_i$ and $\tilde{\sigma}_i^2$ are given by (28)-(29) and [19, eq. 43-44] for the exponential and the Gamma-Gamma distributions of the FSO links, respectively.

Proof. Using the CLT, the random variable $\frac{1}{M_i \tilde{C}_i} \sum_{m=1}^{M_i} \sum_{c=(m-1)\tilde{C}_i+1}^{m\tilde{C}_i} \log \left(1 + \tilde{P}_i \tilde{G}_i(c) \right)$ is approximated by its equivalent Gaussian random variable $\mathcal{R}_i \sim \mathcal{N}(\tilde{\mu}_i, \frac{1}{M_i \tilde{C}_i} \tilde{\sigma}_i^2)$, where for the exponential distribution of the FSO link we have

$$\tilde{\mu}_i = \int_0^\infty f_{\tilde{G}_i}(x) \log \left(1 + \tilde{P}_i x \right) dx \stackrel{(g)}{=} \tilde{P}_i \int_0^\infty \frac{1 - F_{\tilde{G}_i}(x)}{1 + \tilde{P}_i x} dx = -e^{\frac{\lambda_i}{\tilde{P}_i}} \operatorname{Ei} \left(-\frac{\lambda_i}{\tilde{P}_i} \right), \quad (28)$$

and

$$\tilde{\sigma}_i^2 = \tilde{\rho}_i - \tilde{\mu}_i^2,$$

$$\begin{aligned} \tilde{\rho}_i &= \int_0^\infty f_{\tilde{G}_i}(x) \log^2 \left(1 + \tilde{P}_i x \right) dx \stackrel{(h)}{=} 2\tilde{P}_i \int_0^\infty \frac{e^{-\lambda_i x}}{1 + \tilde{P}_i x} \log \left(1 + \tilde{P}_i x \right) dx \stackrel{(i)}{=} \mathcal{H}_i(\infty) - \mathcal{H}_i(1), \\ \mathcal{H}_i(x) &= 2e^{\frac{\lambda_i}{\tilde{P}_i}} \left(\frac{\lambda_i}{\tilde{P}_i} x {}_3F_3 \left(1, 1, 1; 2, 2, 2; -\frac{\lambda_i x}{\tilde{P}_i} \right) \right. \\ &\left. + \frac{1}{2} \log(x) \left(-2 \left(\log \left(\frac{\lambda_i}{\tilde{P}_i} x \right) + \mathcal{E} \right) - 2\Gamma \left(0, \frac{\lambda_i}{\tilde{P}_i} x \right) + \log(x) \right) \right). \end{aligned} \quad (29)$$

Here, $\text{Ei}(x) = \int_x^\infty \frac{e^{-t} dt}{t}$ denotes the exponential integral function. Also, (g) and (h) are obtained by partial integration. Then, denoting the Euler constant by \mathcal{E} , (i) is given by the variable transformation $1 + \tilde{P}_i x = t$, some manipulations, as well as the definition of the Gamma incomplete function $\Gamma(s, x) = \int_x^\infty t^{s-1} e^{-t} dt$ and the generalized hypergeometric function ${}_a F_a(\cdot)$. For the Gamma-Gamma distribution, on the other hand, the PDF $f_{\tilde{G}_i}$ in (28)-(29) is replaced by (5) and the mean and variance are calculated by [19, eq. 43] and [19, eq. 44], respectively. In this way, following the same arguments as in Lemmas 1, 3-4, the outage probability of the FSO-based hops is given by (27). \square

Lemmas 1-5 lead to different corollary statements about the performance of multi-hop RF-FSO systems, as stated in the following.

Corollary 1: With long codewords, there are mappings between the performance of FSO- and RF-based hops, in the sense that the outage probability achieved in an RF-based hop is the same as the outage probability in an FSO-based hop experiencing specific long-term channel characteristics.

Proof. The proof comes from Lemmas 1-5 where for different hops the outage probability is given by the CDF of Gaussian random variables. Thus, with appropriate long-term channel characteristics, (μ_i, σ_i) , $(\hat{\mu}_i, \hat{\sigma}_i)$, $(\check{\mu}_i, \check{\sigma}_i)$ and $(\tilde{\mu}_i, \tilde{\sigma}_i)$ in Lemmas 1 and 3-5 can be equal leading to the same outage probability in these hops. \square

In this way, the performance of RF-FSO based multi-hop/mesh networks can be mapped to ones using only the RF- or the FSO-based communication.

Corollary 2: With asymptotically long codewords,

- 1) the minimum number of transmit antennas in an RF-based hop, such that the same rate is supported in all hops, is found by the solution of

$$\begin{aligned}
N'_i = \arg \left\{ \log \left(1 + \sqrt[1-\vartheta_i]{\frac{\epsilon_i P_i^{\text{cons}}}{(P_i^{\text{max}})^{\vartheta_i}} \left(\frac{-\sqrt{2\pi x \nu_i^2}}{2} + x \zeta_i \right)} \right) \right. \\
+ \mathcal{A}_i \left(\sqrt[1-\vartheta_i]{\frac{\epsilon_i P_i^{\text{cons}}}{(P_i^{\text{max}})^{\vartheta_i}}, \frac{-1}{\sqrt{2\pi x \nu_i^2}}, \frac{1}{2} + \frac{x \zeta_i}{\sqrt{2\pi x \nu_i^2}}, \frac{-\sqrt{2\pi x \nu_i^2}}{2} + x \zeta_i \right) \\
\left. - \mathcal{A}_i \left(\sqrt[1-\vartheta_i]{\frac{\epsilon_i P_i^{\text{cons}}}{(P_i^{\text{max}})^{\vartheta_i}}, \frac{-1}{\sqrt{2\pi x \nu_i^2}}, \frac{1}{2} + \frac{x \zeta_i}{\sqrt{2\pi x \nu_i^2}}, \frac{\sqrt{2\pi x \nu_i^2}}{2} + x \zeta_i \right) = \min_{\forall j=1, \dots, \tilde{T}} \{ \tilde{\mu}_j \} \right\}, \forall i,
\end{aligned} \tag{30}$$

which can be calculated numerically.

2) Also, the ergodic achievable rate of the multi-hop network is approximately given by

$$\bar{C}(T, \tilde{T}) = \min \left(\min_{\forall j=1, \dots, T} \{\check{\mu}_j\}, \min_{\forall j=1, \dots, \tilde{T}} \{\tilde{\mu}_j\} \right), \quad (31)$$

with $\check{\mu}_i$ defined in (24) and $\tilde{\mu}_i$ given by (28) and [19, eq. 43] for the exponential and Gamma-Gamma distributions of the FSO link, respectively.

Proof. With asymptotically long codewords, i.e., very large C_i, \tilde{C}_i , the achievable rates in the RF- and FSO-based hops converge to their corresponding ergodic capacity, and there is no need for HARQ because the data is always correctly decoded if it is transmitted with rates less than or equal to the ergodic capacity. Denoting the expectation operation by $E\{\cdot\}$, the ergodic capacity of an FSO-hop is given by $\tilde{\mu}_i = E\{\log(1 + \tilde{P}_i \tilde{G}_i)\}$ which is determined by (28) and [19, eq. 43] for the exponential and Gamma-Gamma distributions of the FSO-based hop, respectively. For the RF-based hop, on the other hand, the ergodic capacity is found as $E\left\{\log\left(1 + \sqrt[1-\vartheta_i]{\frac{c_i P_i^{\text{cons}}}{(P_i^{\text{max}})^{\vartheta_i}} G_i}\right)\right\} \simeq \check{\mu}_i$ with $\check{\mu}_i$ given in (24). In this way, the maximum achievable rate of the FSO-based hops is $\tilde{R} = \min_{\forall j=1, \dots, \tilde{T}} \{\tilde{\mu}_j\}$. Also, the minimum number of required antennas in the i -th RF-based hop is found by solving $\check{\mu}_i = \tilde{R}$ which, from (24), leads to (30). Note that (30) is a single-variable equation and can be effectively solved by different numerical techniques.

Finally, following the same argument, the ergodic achievable rate of the RF-FSO network is given by (31), i.e., the maximum rate in which the data is correctly decoded in all hops. \square

B. Performance Analysis with Short Codewords

Up to now, we considered the long-codeword scenario such that the CLT provides accurate approximation for the sum of independent and identically distributed (IID) random variables. However, it is interesting to analyze the system performance in cases with short codewords, i.e., when C_i and $\tilde{C}_i, \forall i$, are small. This case is especially important for FSO links since the coherence time can be quite long (milliseconds). Here, we mainly concentrate on the Gamma-Gamma distribution of the FSO-based hops. The same results as in [45] can be applied to derive the outage probability of the FSO-based hops in the cases with exponential distribution.

Lemma 6: For arbitrary numbers of M_i, C_i and \tilde{C}_i ,

- 1) The outage probabilities of the FSO- and RF-based hops are bounded by (33) and (36), respectively.

- 2) At low SNRs, a MISO-HARQ RF-based hop with M_i retransmissions, N_i transmit antennas and C_i channel realizations per sub-codeword transmission can be mapped to an open-loop MISO setup with $M_i N_i C_i$ transmit antennas and single channel realization per codeword transmission.

Proof. Considering the FSO-based hops, one can use the Minkowski inequality [46, Theorem 7.8.8]

$$\left(1 + \left(\prod_{i=1}^n x_i\right)^{\frac{1}{n}}\right)^n \leq \prod_{i=1}^n (1 + x_i), \quad (32)$$

to write

$$\begin{aligned} \tilde{\phi}_i &= \Pr \left(\frac{1}{M_i \tilde{C}_i} \sum_{m=1}^{M_i} \sum_{c=(m-1)\tilde{C}_i+1}^{m\tilde{C}_i} \log(1 + \tilde{P}_i \tilde{G}_i(c)) \leq \frac{R_i}{M_i} \right) \\ &= \Pr \left(\prod_{m=1}^{M_i} \prod_{c=(m-1)\tilde{C}_i+1}^{m\tilde{C}_i} (1 + \tilde{P}_i \tilde{G}_i(c)) \leq e^{\tilde{C}_i R_i} \right) \\ &\leq \Pr \left(1 + \tilde{P}_i \left(\prod_{m=1}^{M_i} \prod_{c=(m-1)\tilde{C}_i+1}^{m\tilde{C}_i} \tilde{G}_i(c) \right)^{\frac{1}{M_i \tilde{C}_i}} \leq e^{\frac{R_i}{M_i}} \right) = F_{\mathcal{J}_i} \left(\left(\frac{e^{\frac{R_i}{M_i}} - 1}{\tilde{P}_i} \right)^{M_i \tilde{C}_i} \right), \quad (33) \end{aligned}$$

where, using the results of [42, Lemma 3] and for the Gamma-Gamma distribution of the variables \tilde{G}_i , the random variable $\mathcal{J}_i = \prod_{m=1}^{M_i} \prod_{c=(m-1)\tilde{C}_i+1}^{m\tilde{C}_i} \tilde{G}_i(c)$ follows the CDF

$$F_{\mathcal{J}_i}(x) = \frac{1}{\Gamma^{M_i \tilde{C}_i}(a_i) \Gamma^{M_i \tilde{C}_i}(b_i)} \mathcal{G}_{1,2}^{2M_i \tilde{C}_i, 1} \left((a_i b_i)^{M_i \tilde{C}_i} x \left| \begin{matrix} 1 \\ \underbrace{a_i, a_i, \dots, a_i}_{M_i \tilde{C}_i \text{ times}}, \underbrace{b_i, b_i, \dots, b_i}_{M_i \tilde{C}_i \text{ times}}, 0 \end{matrix} \right. \right), \quad (34)$$

with $\mathcal{G}(\cdot)$ denoting the Meijer G-function. Note that, the results of (33) are mathematically applicable for every values of M_i, \tilde{C}_i . However, for, say $M_i \tilde{C}_i \geq 6$, the implementation of the Meijer G-function in MATLAB is very time-consuming and the tightness of the approximation decreases with M_i, \tilde{C}_i . Therefore, (33) is useful for the performance analysis in cases with small $M_i, \tilde{C}_i, \forall i$, while the CLT-based approach of Section III.A provides accurate performance evaluation for cases with long codewords.

For the RF-based hop, on the other hand, we use

$$\frac{1}{n} \log \left(1 + \sum_{j=1}^n x_j \right) \leq \frac{1}{n} \sum_{j=1}^n \log(1 + x_j) \leq \log \left(1 + \frac{1}{n} \sum_{j=1}^n x_j \right), \forall n, x_j \geq 0, \quad (35)$$

to lower- and upper-bound the outage probability by

$$\begin{aligned}
& \Pr \left(\log \left(1 + \frac{1-\vartheta_i \sqrt{\frac{\epsilon_i P_i^{\text{cons}}}{(P_i^{\text{max}})^{\vartheta_i}}}}{M_i C_i} \sum_{m=1}^{M_i} \sum_{c=(m-1)C_i+1}^{mC_i} G_i(c) \right) \leq \frac{R_i}{M_i} \right) \\
& \leq \phi_i \leq \Pr \left(\frac{1}{M_i C_i} \log \left(1 + 1-\vartheta_i \sqrt{\frac{\epsilon_i P_i^{\text{cons}}}{(P_i^{\text{max}})^{\vartheta_i}}} \sum_{m=1}^{M_i} \sum_{c=(m-1)C_i+1}^{mC_i} G_i(c) \right) \leq \frac{R_i}{M_i} \right) \\
& \Rightarrow F_{\mathbf{G}_i} \left(\frac{M_i C_i \left(e^{\frac{R_i}{M_i}} - 1 \right)}{1-\vartheta_i \sqrt{\frac{\epsilon_i P_i^{\text{cons}}}{(P_i^{\text{max}})^{\vartheta_i}}}} \right) \leq \phi_i \leq F_{\mathbf{G}_i} \left(\frac{e^{R_i C_i} - 1}{1-\vartheta_i \sqrt{\frac{\epsilon_i P_i^{\text{cons}}}{(P_i^{\text{max}})^{\vartheta_i}}}} \right). \tag{36}
\end{aligned}$$

Here, $\mathbf{G}_i = \sum_{m=1}^{M_i} \sum_{c=(m-1)C_i+1}^{mC_i} \sum_{j_i=1}^{N_i} g_i^{j_i}(c)$ is an equivalent sum channel gain variable with $M_i C_i N_i$ antennas at the transmitter whose PDF is obtained by replacing N_i with $M_i C_i N_i$ in (2). Also, $F_{\mathbf{G}_i}(\cdot)$ denotes the CDF of the equivalent sum channel gain variable.

To prove Lemma 6 part 2, we note that letting $x_i \rightarrow 0, \forall i$, the inequalities in (35) are changed to equality. Thus, as a corollary result, at low SNRs a MISO-HARQ RF-link with N_i transmit antennas, M_i retransmissions and C_i channel realizations within each retransmission round can be mapped to an open-loop MISO setup with $M_i C_i N_i$ transmit antennas, in the sense that the same outage probability is achieved in these setups. \square

Note that the bounding schemes of (36) are mathematically applicable for every values of M_i, C_i . However, while the results of (36) tightly match the exact numerical results for small values of M_i, C_i , the tightness decreases for large M_i, C_i 's. Thus, the results of Lemmas 1-4 and Lemma 6 can be effectively applied for the performance analysis of the RF-based hops in the cases with long and short codewords, respectively. Finally, as another approximation for the cases with $M_i = 1, C_i = 1$, we have

$$\phi_{i|M_i=1, C_i=1} \simeq \frac{1}{2} \left(1 + \operatorname{erf} \left(\frac{\left(\frac{e^{R_i} - 1}{1-\vartheta_i \sqrt{\frac{\epsilon_i P_i^{\text{cons}}}{(P_i^{\text{max}})^{\vartheta_i}}}} - N_i \zeta_i \right)}{\sqrt{2N_i \nu_i^2}} \right) \right), \tag{37}$$

which comes from Lemma 2.

C. Performance Analysis in Mesh Networks

Consider a mesh network consisting of \mathcal{X} non-overlapping routes from the source to the destination with independent channel realizations for the hops. The ξ -th, $\xi = 1, \dots, \mathcal{X}$, route is

made of T_ξ RF- and \tilde{T}_ξ FSO-based hops and the routes can have different total number of hops $T_\xi^{\text{total}} = T_\xi + \tilde{T}_\xi, \xi = 1, \dots, \mathcal{X}$. In this case, the network outage probability is given by

$$\Pr(\text{Outage})^{\text{mesh}} = \prod_{\xi=1}^{\mathcal{X}} (\Pr(\text{Outage}_\xi)), \quad (38)$$

where $\Pr(\text{Outage}_\xi)$ is the outage probability in the ξ -th route as given in (6). In (38), we have used the fact that in a mesh network an outage occurs if the data is correctly transferred to the destination through none of the routes. With the same arguments, the ergodic achievable rate of the mesh network is obtained by

$$\bar{C}^{\text{mesh}} = \max_{\forall \xi=1, \dots, \mathcal{X}} \{\bar{C}_\xi\}, \quad (39)$$

with \bar{C}_ξ derived in (31). This is based on the fact that, knowing the long-term channel characteristics, one can set the data rate equal to the maximum achievable rate of the best route and the message is always correctly decoded by the destination, if the codewords are asymptotically long. The performance of mesh networks is studied in Fig. 9.

IV. NUMERICAL RESULTS

Throughout the paper, we presented different approximation techniques. The verification of these results is demonstrated in Figs. 1, 2, 6-8 and, as seen in the sequel, the analytical results follow the numerical results with high accuracy. Then, to avoid too much information in each figure, Figs. 3-5, 9 report only the simulation results. Note that in all figures we have double-checked the results with the ones obtained analytically, and they match tightly.

The simulation results are presented for homogenous setups. That is, different RF-based hops follow the same long-term fading parameters $K_i, \omega_i, \forall i$, in (1)-(2), and the FSO-based hops also experience the same long-term channel parameters, i.e., λ_i, a_i and b_i in (4)-(5). Moreover, we set $M_i = M_j$ and $R_i = R_j, \forall i, j = 1, \dots, T^{\text{total}}$. In all figures, we set $\tilde{P}_i = N_i P_i^{\text{cons}}$ such that the total consumed power at different hops is the same. Then, using (3), one can determine the output power of the RF-based antennas. Also, because the noise variances are set to 1, \tilde{P}_i (in dB, $10 \log_{10} \tilde{P}_i$) is referred to the SNR as well. In Figs. 1, 2 and 5, we assume an ideal PA. The effect of non-ideal PAs is verified in Figs. 3, 4, 6-9. With non-ideal PAs, we consider the state-of-the-art parameter settings $\vartheta_i = 0.5, \epsilon_i = 0.75, P_i^{\text{max}} = 25$ dB, $\forall i$, [34]–[37], unless otherwise stated.

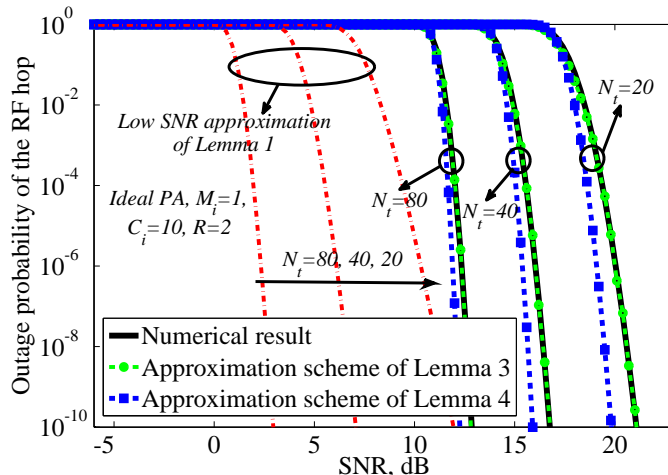


Figure 1. On the tightness of the results in Lemmas 1-4. Ideal PA, single RF-based hop, $M_i = 1$, $R = 2$, $C_i = 10$. The results are presented for $N_i = 20, 40$, and $80, \forall i$.

The parameters of the Rician RF PDF (1) are set to $\omega_i = 1$, $K_i = 0.01, \forall i$, leading to unit mean and variance of the channel gain distribution $f_{g_i^{j_i}}(x), \forall i, j_i$. With the exponential distribution of the FSO-based hops, we consider $f_{\tilde{G}_i}(x) = \lambda_i e^{-\lambda_i x}$ with $\lambda_i = 1, \forall i$. Also, for the Gamma-Gamma distribution we set $f_{\tilde{G}_i}(x) = \frac{2(a_i b_i)^{\frac{a_i + b_i}{2}}}{\Gamma(a_i)\Gamma(b_i)} x^{\frac{a_i + b_i}{2} - 1} \mathcal{K}_{a_i - b_i}(2\sqrt{a_i b_i x})$, $a_i = 4.3939, b_i = 2.5636, \forall i$, which corresponds to Rytov variance of 1 [42]. Figures 1-8 consider multi-hop networks. The performance of mesh networks is studied in Fig. 9. Note that, as discussed in Section III, the results of cases with long codewords and few number of retransmissions can be mapped to the cases with short codewords, large number of retransmissions and a scaled code rate (see (7)-(8)). Finally, it is worth noting that we have verified the analytical and the numerical results for a broad range of parameter settings, which, due to space limits and because they lead to the same qualitative conclusions as in the presented figures, are not reported in the figures.

The simulation results are presented in different parts as follows.

On the approximation approaches of Lemmas 1-5: Considering an ideal PA, $M_i = 1$ (as the worst-case scenario), $R_i = 2$ npcu, and $C_i = 10, \forall i$, Fig. 1 verifies the tightness of the approximation schemes of Lemmas 1-4. Particularly, we plot the outage probability of an RF-based hop for different numbers of transmit antennas $N_i, \forall i$. Then, Fig. 2 demonstrates the outage probability of a dual-hop RF-FSO setup versus the SNR. Here, we set $M_i = 1, R_i = 1, 2$ npcu, and $C_i = 10, \tilde{C}_i = 30, N_i = 20, T = 1, \tilde{T} = 1 \forall i$, and the results are presented for cases with ideal PAs at the RF-based hops. As observed, the analytical results of Lemmas 2-5 mimic the exact results with very high accuracy (Figs. 1-2). Also, Lemma 1 properly approximates the

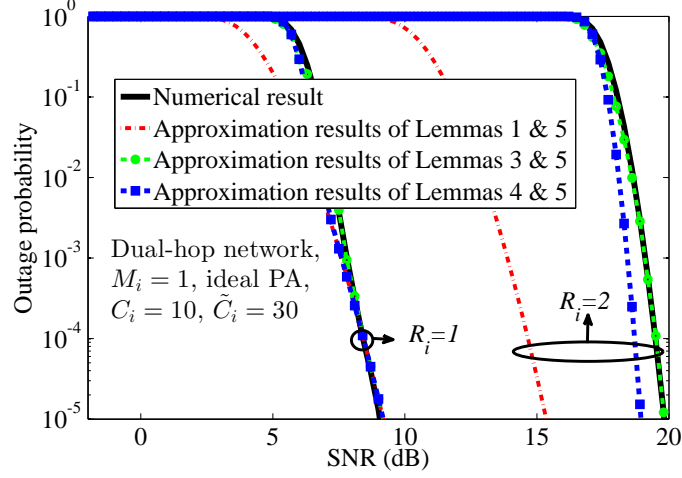


Figure 2. On the tightness of the results in Lemmas 1-5. Ideal PA, dual-hop network, $M_i = 1$, $R_i = 1, 2$, $C_i = 10$, $\tilde{C}_i = 30$, $T = 1$, $\tilde{T} = 1$, and $N_i = 20$, $\forall i$.

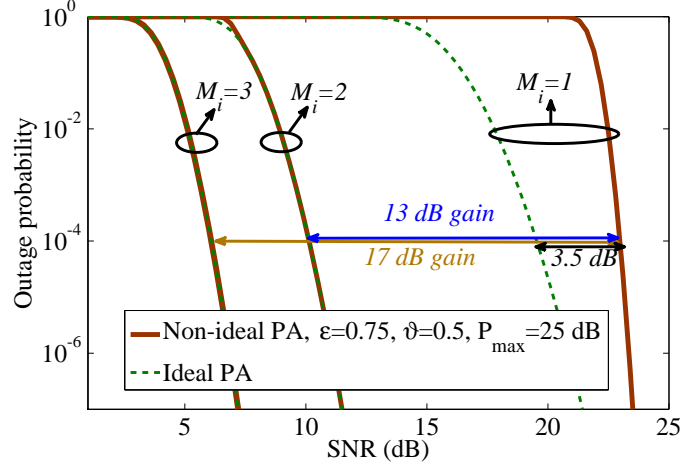


Figure 3. Outage probability of a dual-hop RF-FSO network for different PA models and maximum number of retransmissions, M_i , $\forall i$. Exponential distribution of the FSO link, $T = 1$, $\tilde{T} = 1$, $C_i = 10$, $\tilde{C}_i = 20$, $R_i = 3$ npcu, and $N_i = 60$, $\forall i$.

outage probability at low and high SNRs, and the tightness increases as the code rate decreases (Fig. 2). Moreover, the tightness of the approximation results of Lemmas 3-4 increases with the number of RF-based transmit antennas (Fig. 1). This is because the tightness of the CLT-based approximations in Lemma 2 increases with N_i , $\forall i$. Finally, although not demonstrated in Figs. 1-2, the tightness of the CLT-based approximation schemes of Lemmas 3-5 increases with the maximum number of retransmissions M_i , $\forall i$.

On the effect of HARQ and imperfect PAs: Shown in Fig. 3 is the outage probability of a dual-hop RF-FSO network for different maximum numbers of HARQ-based retransmission rounds M_i , $\forall i$. Also, the figure compares the system performance in cases with ideal and non-ideal PAs. Here, the results are obtained for the exponential distribution of the FSO link, $T = 1$, $\tilde{T} =$

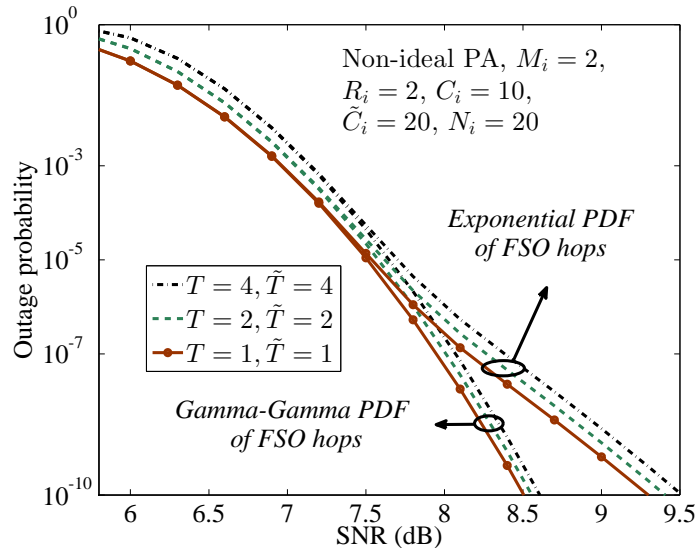


Figure 4. The outage probability for different numbers of RF- and FSO-based hops, i.e., T and \tilde{T} . Non-ideal PA, $\vartheta_i = 0.5$, $\epsilon_i = 0.75$, $P_i^{\max} = 25$ dB, $M_i = 2$, $N_i = 20$, $R_i = 2$ npcu, $C_i = 10$, and $\tilde{C}_i = 20$, $\forall i$.

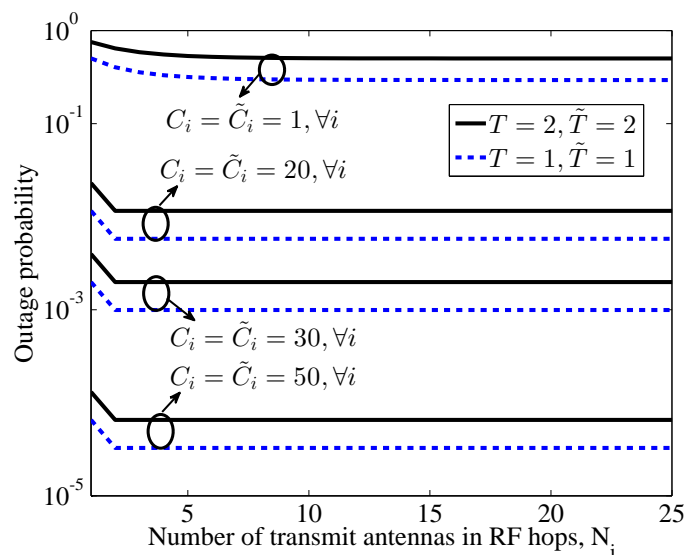


Figure 5. Outage probability for different numbers of transmit antennas in the RF-based hops and channel coherence times. Exponential distribution of the FSO-based hops, ideal PA, $R_i = 1.5$ npcu, $M_i = 1$, $T_i = \tilde{T}_i = 1$, $\forall i$, and SNR = 10 dB.

1, $C_i = 10$, $\tilde{C}_i = 20$, $R_i = 3$ npcu, and $N_i = 60$, $\forall i$. As demonstrated, with no HARQ, the efficiency of the RF-based PAs affects the system performance considerably. For instance, with the parameter settings of the figure and outage probability 10^{-4} , the PAs inefficiency increases the required power by 3.5 dB. On the other hand, the HARQ can effectively compensate the effect of imperfect PAs, and the difference between the outage probability of the cases with ideal and non-ideal PAs is negligible for $M > 1$. Also, the effect of non-ideal PA decreases at high

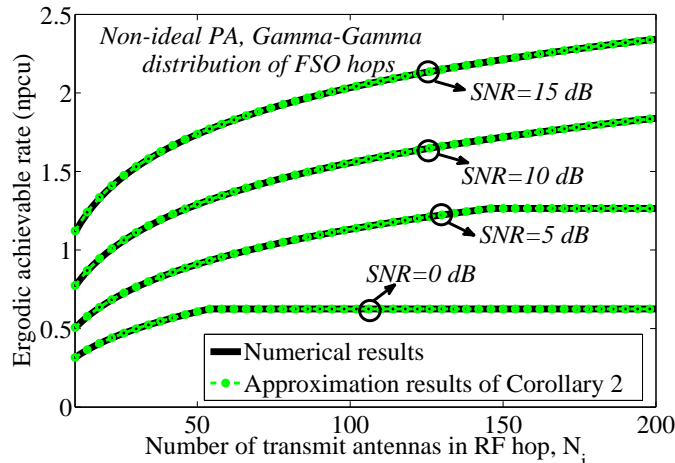


Figure 6. Ergodic achievable rate for different numbers of transmit antennas in the RF-based hops and SNRs. Gamma-Gamma distribution of the FSO-based hops, non-ideal PA $\vartheta_i = 0.5$, $\epsilon_i = 0.75$, and $P_i^{\max} = 25$ dB, $\forall i$.

SNRs which is intuitively because the *effective* efficiency of the PAs $\epsilon_i^{\text{effective}} = \epsilon_i \left(\frac{P_i}{P_i^{\max}}\right)^{\vartheta_i}$, $\forall i$, is improved as the SNR increases. Finally, the implementation of HARQ improves the energy efficiency significantly. As an example, consider the outage probability 10^{-4} , an ideal PA and the parameter settings of Fig. 3. Then, compared to the open-loop communication, i.e., $M_i = 1$, the implementation of HARQ with a maximum of 2 and 3 retransmissions reduces the required power by 13 and 17 dB, respectively.

System performance with different numbers of hops: In Fig. 4, we demonstrate the outage probability in cases with different numbers of RF- and FSO-based hops, i.e., T, \tilde{T} . In harmony with intuition, the outage probability increases with the number of hops. However, the outage probability increment is negligible, particularly at high SNRs, because the data is correctly decoded with high probability in different hops as the SNR increases. Finally, as a side result, the figure indicates that the outage probability of the RF-FSO based multi-hop network is not sensitive to the distribution of the FSO-based hops at low SNRs. This is intuitive because, at low SNRs and with the parameter settings of the figure, the outage event mostly occurs in the RF-based hops. However, at high SNRs where the outage probability of different hops are comparable, the PDF of the FSO-based hops affects the network performance.

On the effect of RF-based transmit antennas: Considering an exponential distribution of the FSO-based hops, ideal PAs, $R_i = 1.5$ npcu, $M_i = 1$, $T_i = \tilde{T}_i = 1$, $\forall i$, and SNR = 10 dB, Fig. 5 demonstrates the effect of the number of RF transmit antennas on the network outage probability. Also, the figure compares the system performance in cases with short and long

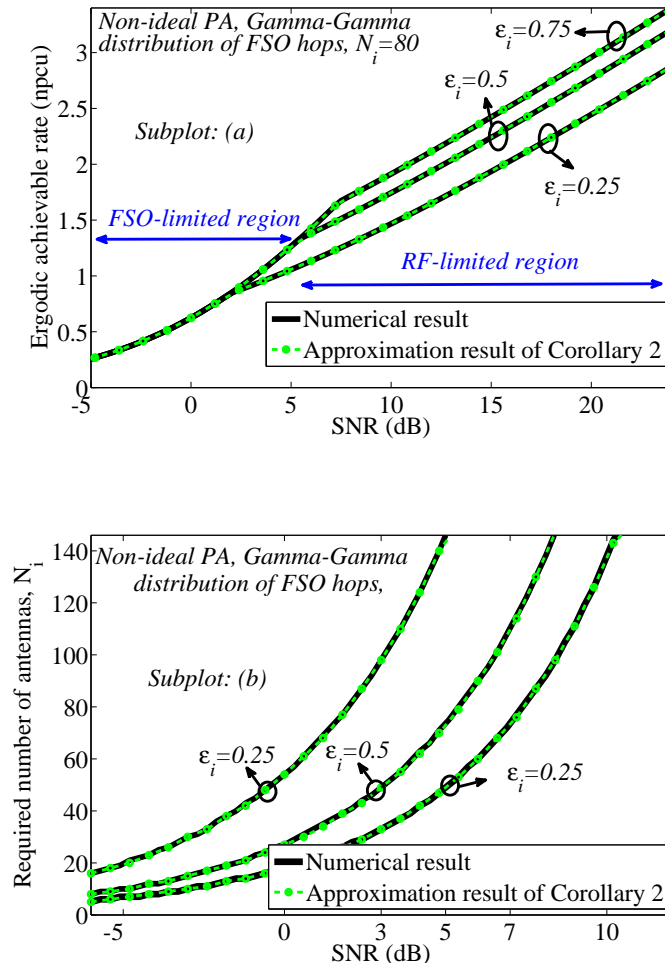


Figure 7. On the tightness of the analytical results of Corollary 2. Subplot (a): Ergodic achievable rate vs the SNR. Non-ideal PA, Gamma-Gamma distribution of the FSO hops, $N_i = 80, \forall i$. Subplot (b): The minimum number of transmit antennas in the RF-based hops to guarantee the same rate as in the FSO-based hops. Non-ideal PA and Gamma-Gamma distribution of the FSO hops. For the non-ideal PAs, we have $\vartheta_i = 0.5, \epsilon_i = 0.75$, and $P_i^{\max} = 25$ dB, $\forall i$.

codewords, i.e., in cases with small and large values of C_i, \tilde{C}_i . As seen, with short codewords, the outage probability decreases with the number of RF-based transmit antennas monotonically. This is because, with the parameter settings of the figure, the data is correctly decoded with higher probability as the number of antennas increases. With long codewords, on the other hand, the outage probability is (almost) insensitive to the number of transmit antennas for $N_i \geq 3$. Finally, the outage probability decreases with C_i, \tilde{C}_i , because the HARQ exploits time diversity as more channel realizations are experienced within each codeword transmission.

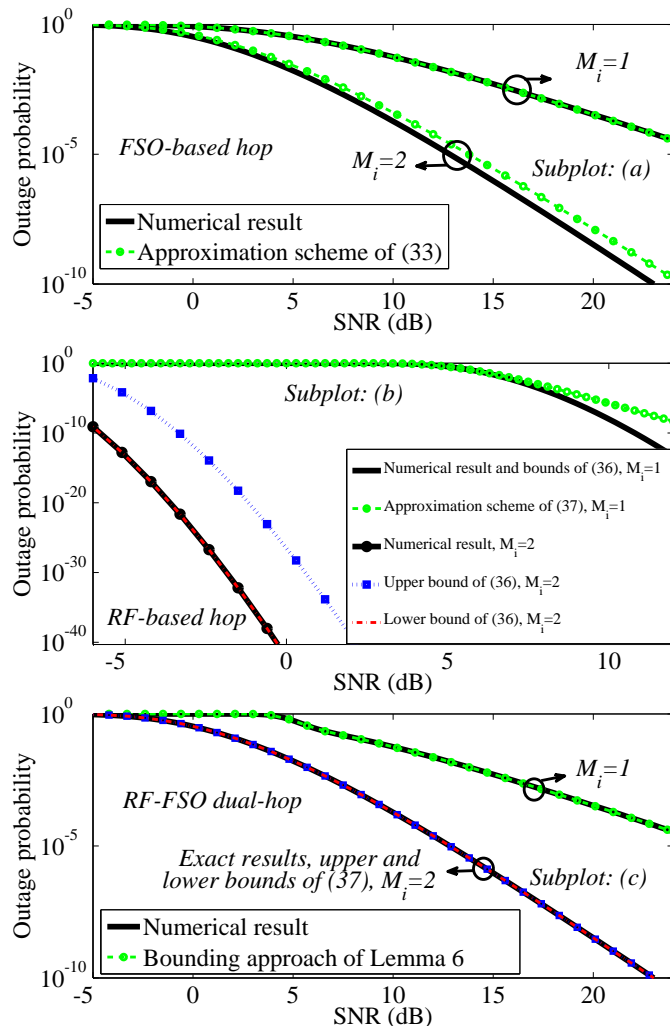


Figure 8. Outage probability in the cases with short codewords. Non-ideal PA, Gamma-Gamma distribution of the FSO hops, $R_i = 1$ npcu, $M_i = 1$, $C_i = 1$, $\tilde{C}_i = 1$, $N_i = 60$, $\forall i$. For the non-ideal PAs, we have $\vartheta_i = 0.5$, $\epsilon_i = 0.75$, and $P_i^{\max} = 25$ dB, $\forall i$. In subplots a-c, the outage probability is presented for an FSO-based hop, an RF-based hop and a dual-hop RF-FSO network, respectively.

In Fig. 6, we plot the network ergodic achievable rates for cases with Gamma-Gamma distribution of the FSO-based hops, non-ideal PAs and different numbers of transmit antennas/SNRs. Also, the figure verifies the accuracy of the approximation schemes of Corollary 2. Note that, due to the homogenous network structure, the ergodic rate is independent of the number of RF- and FSO-based hops. As seen, at low/moderate SNRs, the network ergodic rate increases (almost) logarithmically with the number of RF antennas. At high SNRs, on the other hand, the ergodic rate becomes independent of the number of RF transmit antennas. This is because with

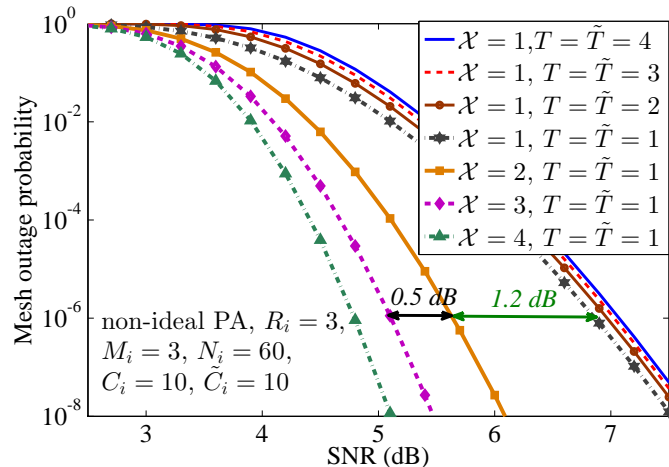


Figure 9. Outage probability of a mesh network for different numbers of routes and hops. Non-ideal PA, Gamma-Gamma distribution of the FSO hops, $R_i = 3$ npcu, $M_i = 3$, $C_i = 10$, $\tilde{C}_i = 10$, and $N_i = 60$, $\forall i$. For the non-ideal PAs, we have $\vartheta_i = 0.5$, $\epsilon_i = 0.75$, and $P_i^{\max} = 25$ dB, $\forall i$.

large number of RF-based antennas the achievable rate of the RF-based hops exceeds the one in FSO-based hops, and the network ergodic rate is given by the achievable rate of the FSO-based hops. Finally, the number of antennas above which the ergodic rate is limited by the achievable rate of the FSO-based hops increases with the SNR.

On the ergodic achievable rates: Along with Fig. 6, we evaluate the accuracy of the results of Corollary 2 in Figs. 7a and 7b. Particularly, Fig. 7a demonstrates the network ergodic rate for different PA models and compares the simulation results with the ones derived in (31). Then, Fig. 7b verifies the accuracy of (30). Here, we show the minimum number of required RF transmit antennas versus the SNR which determines the ergodic rate of the FSO-based hops. As can be seen, the approximation results of Corollary 2 are very tight for a broad range of parameter settings. Thus, (30) and (31) can be effectively used to derive the required number of RF transmit antennas and the network ergodic rate, respectively (Figs. 7a and 7b). The ergodic rate shows different behaviors in the, namely, FSO-limited and RF-limited regions. With the parameter settings of the figure, the ergodic rate is limited by the achievable rates of the FSO-based hops at low SNRs (FSO-limited region in Fig. 7a). However, as the SNR increases, the achievable rates of the FSO-based hops exceed the ones in the RF-based hops and, consequently, the network ergodic rate is limited by the rate of the RF-based hops (RF-limited region in Fig. 7a). As a result, the efficiency of the RF PAs affects the ergodic rate at high SNRs. Finally, the figure indicates that at high SNRs the network ergodic rate increases (almost) linearly with the SNR.

As shown in Fig. 7b, the required number of RF-based transmit antennas to guarantee the same rate as in the FSO-based hops increases considerably with the SNR and, consequently, the ergodic rate of the FSO-based hops. Moreover, the PAs efficiency affects the required number of antennas significantly. As an example, consider the parameter settings of Fig. 7b and SNR = 3 dB. Then, the required number of RF-based antennas is given by 33, 49 and 98 for the cases with PA efficiency 75%, 50% and 25%, respectively. Thus, hardware impairments such as the PA inefficiency affect the system performance remarkably and should be carefully considered in the network design. However, selecting the proper number of antennas and PA properties is not easy because the decision depends on several parameters such as complexity, infrastructure size and cost.

Performance analysis with short codewords: In Figs. 8a, 8b and 8c, we study the outage probability of an FSO-based hop, an RF-based hop and a dual-hop RF-FSO network, respectively. Particularly, considering non-ideal PAs and Gamma-Gamma distribution of the FSO-based hops, the results are obtained for $C_i = \tilde{C}_i = 1$, $M_i = 1, 2 \forall i$, and we evaluate the accuracy of different bounds/approximations in Lemma 6 and (37). As demonstrated, the bound of (33) matches the exact values derived via simulation analysis of $\tilde{\phi}_i$ exactly in cases with $M_i = 1$. Also, the bounding/approximation methods of (33), (36) and (37) mimic the numerical results with high accuracy in cases with a maximum of $M_i = 2, \forall i$, retransmissions. Thus, the results of Section III.B can be efficiently used to analyze the RF-FSO systems in cases with small values of $M_i, C_i, \tilde{C}_i, \forall i$.

On the performance of mesh networks: In Fig. 9, we study the outage probability of mesh networks for different numbers of routes. Here, we consider non-ideal PAs, exponential PDF of the FSO hops, $M_i = 3$, $N_i = 60$, $C_i = 10$, $\tilde{C}_i = 10$, and $R_i = 3$ npcu. The results are presented for cases with one RF- and one FSO-based hop in each route. Also, we compare the outage probability of the mesh network with that of a single route setup consisting of different numbers of RF- and FSO-based hops. Note that there are the same total number of RF- and FSO-based hops in each case with $\mathcal{X} = n, T_{\S} = \tilde{T}_{\S} = 1, \forall \S = 1, \dots, \mathcal{X}$, and $\mathcal{X} = 1, T_1 = \tilde{T}_1 = n$.

As demonstrated in Fig. 9, in contrast to the single-route setup where the outage probability increases with the number of hops, the outage probability of the mesh network decreases considerably by adding more parallel routes into the network. For instance, consider the parameter settings of the figure and outage probability of 10^{-6} . Then, compared to cases with a single route, the required SNR at each hop decreases by almost 1.2 dB if the data is transferred through

two routes. This is intuitive because the probability that the data is correctly received by the destination increases with the number of routes. However, the relative effect of adding more routes decreases with the number of routes, and, for the example parameters considered, there is about 0.5 dB energy efficiency improvement if the number of routes increases from $\mathcal{X} = 2$ to $\mathcal{X} = 3$. Finally, while we did not consider it in Section III.C, the performance of the mesh network is further improved if the signals from different routes are combined at the destination.

V. CONCLUSION

We studied the performance of RF-FSO based multi-hop and mesh networks in cases with short and long codewords. Considering different channel conditions, we derived closed-form expressions for the networks outage probability, the ergodic rates as well as the required number of RF transmit antennas to guarantee different achievable rate quality-of-service requirements. The results are presented for cases with and without HARQ. As demonstrated, depending on the codeword length, there are different methods for analytical performance evaluation of the multi-hop/mesh networks. Moreover, there are mappings between the performance of RF-FSO based multi-hop networks and the ones using only the RF- or the FSO-based communication. Also, the HARQ can effectively improve the energy efficiency and compensate for the effect of hardware impairments. Finally, the outage probability of multi-hop networks is not sensitive to the large number of RF-based transmit antennas while the ergodic rate is significantly affected by the number of antennas.

ACKNOWLEDGEMENT

The research leading to these results received funding from the European Commission H2020 programme under grant agreement $n^{\circ}671650$ (5G PPP mmMAGIC project), and from the Swedish Governmental Agency for Innovation Systems (VINNOVA) within the VINN Excellence Center Chase.

REFERENCES

- [1] A. Vavoulas, H. G. Sandalidis, and D. Varoutas, "Weather effects on FSO network connectivity," *IEEE J. Opt. Commun. Netw.*, vol. 4, no. 10, pp. 734–740, Oct. 2012.
- [2] L. Yang, X. Gao, and M.-S. Alouini, "Performance analysis of relay-assisted all-optical FSO networks over strong atmospheric turbulence channels with pointing errors," *J. Lightw. Technol.*, vol. 32, no. 23, pp. 4011–4018, Dec. 2014.

- [3] M. Usman, H. C. Yang, and M.-S. Alouini, "Practical switching-based hybrid FSO/RF transmission and its performance analysis," *IEEE Photon. J.*, vol. 6, no. 5, pp. 1–13, Oct. 2014.
- [4] F. Nadeem, B. Flecker, E. Leitgeb, M. S. Khan, M. S. Awan, and T. Javornik, "Comparing the fog effects on hybrid network using optical wireless and GHz links," in *Proc. IEEE CNSDSP'2008*, Graz, Austria, July 2008, pp. 278–282.
- [5] H. Wu, B. Hamzeh, and M. Kavehrad, "Achieving carrier class availability of FSO link via a complementary RF link," in *Proc. IEEE Asilomar'2004*, California, USA, Nov. 2004, pp. 1483–1487.
- [6] Z. Jia, F. Ao, and Q. Zhu, "BER performance of the hybrid FSO/RF attenuation system," in *Proc. IEEE ISAPE'2006*, Guilin, China, Oct. 2006, pp. 1–4.
- [7] T. Kamalakis, I. Neokosmidis, A. Tsipouras, S. Pantazis, and I. Andrikopoulos, "Hybrid free space optical/millimeter wave outdoor links for broadband wireless access networks," in *Proc. IEEE PIMRC'2007*, Athens, Greece, Sept. 2007, pp. 1–5.
- [8] H. Wu, B. Hamzeh, and M. Kavehrad, "Availability of airbourne hybrid FSO/RF links," in *Proc. SPIE*, 2005, vol. 5819.
- [9] Y. Tang and M. Brandt-Pearce, "Link allocation, routing and scheduling of FSO augmented RF wireless mesh networks," in *Proc. IEEE ICC'2012*, Ottawa, Canada, June 2012, pp. 3139–3143.
- [10] A. Sharma and R. S. Kaler, "Designing of high-speed inter-building connectivity by free space optical link with radio frequency backup," *IET Commun.*, vol. 6, no. 16, pp. 2568–2574, Nov. 2012.
- [11] K. Kumar and D. K. Borah, "Hybrid FSO/RF symbol mappings: Merging high speed FSO with low speed RF through BICM-ID," in *Proc. IEEE GLOBECOM'2012*, California, USA, Dec. 2012, pp. 2941–2946.
- [12] N. Letzepis, K. D. Nguyen, A. Guillen i Fabregas, and W. G. Cowley, "Outage analysis of the hybrid free-space optical and radio-frequency channel," *IEEE J. Sel. Areas Commun.*, vol. 27, no. 9, pp. 1709–1719, Dec. 2009.
- [13] S. Vangala and H. Pishro-Nik, "A highly reliable FSO/RF communication system using efficient codes," in *Proc. IEEE GLOBECOM'2007*, Washington, DC, USA, Nov. 2007, pp. 2232–2236.
- [14] I. B. Djordjevic, B. Vasic, and M. A. Neifeld, "Power efficient LDPC-coded modulation for free-space optical communication over the atmospheric turbulence channel," in *Proc. OFC/NFOEC'2007*, Anaheim, CA, USA, March 2007, pp. 1–3.
- [15] Y. Tang, M. Brandt-Pearce, and S. G. Wilson, "Link adaptation for throughput optimization of parallel channels with application to hybrid FSO/RF systems," *IEEE Trans. Commun.*, vol. 60, no. 9, pp. 2723–2732, Sept. 2012.
- [16] B. He and R. Schober, "Bit-interleaved coded modulation for hybrid RF/FSO systems," *IEEE Trans. Commun.*, vol. 57, no. 12, pp. 3753–3763, Dec. 2009.
- [17] A. Abdulhussein, A. Oka, T. T. Nguyen, and L. Lampe, "Rateless coding for hybrid free-space optical and radio-frequency communication," *IEEE Trans. Wireless Commun.*, vol. 9, no. 3, pp. 907–913, March 2010.
- [18] J. Perez-Ramirez and D. K. Borah, "Design and analysis of bit selections in HARQ algorithm for hybrid FSO/RF channels," in *Proc. IEEE VTC Spring'2013*, Dresden, Germany, June 2013, pp. 1–5.
- [19] B. Makki, T. Svensson, T. Eriksson, and M. S. Alouini, "On the performance of RF-FSO links with and without hybrid ARQ," *IEEE Trans. Wireless Commun.*, vol. 15, no. 7, pp. 4928–4943, July 2016.
- [20] K. Kumar and D. K. Borah, "Relaying in fading channels using quantize and encode forwarding through optical wireless links," in *IEEE GLOBECOM'2013*, Atlanta, GA, USA, Dec. 2013, pp. 3741–3747.
- [21] —, "Quantize and encode relaying through FSO and hybrid FSO/RF links," *IEEE Trans. Veh. Technol.*, vol. 64, no. 6, pp. 2361–2374, June 2015.
- [22] H. Samimi and M. Uysal, "End-to-end performance of mixed RF/FSO transmission systems," *IEEE/OSA Journal of Optical Communications and Networking*, vol. 5, no. 11, pp. 1139–1144, Nov. 2013.
- [23] E. Lee, J. Park, D. Han, and G. Yoon, "Performance analysis of the asymmetric dual-hop relay transmission with mixed RF/FSO links," *IEEE Photon. Technol. Lett.*, vol. 23, no. 21, pp. 1642–1644, Nov. 2011.

- [24] E. Zedini, I. S. Ansari, and M. S. Alouini, "Unified performance analysis of mixed line of sight RF-FSO fixed gain dual-hop transmission systems," in *Proc. IEEE WCNC'15*, New Orleans, LA, USA, March 2015, pp. 46–51.
- [25] I. S. Ansari, F. Yilmaz, and M. S. Alouini, "Impact of pointing errors on the performance of mixed RF/FSO dual-hop transmission systems," *IEEE Wireless Commun. Lett.*, vol. 2, no. 3, pp. 351–354, June 2013.
- [26] J. Zhang, L. Dai, Y. Zhang, and Z. Wang, "Unified performance analysis of mixed radio frequency/free-space optical dual-hop transmission systems," *J. Lightw. Technol.*, vol. 33, no. 11, pp. 2286–2293, June 2015.
- [27] N. I. Miridakis, M. Matthaiou, and G. K. Karagiannidis, "Multiuser relaying over mixed RF/FSO links," *IEEE Trans. Commun.*, vol. 62, no. 5, pp. 1634–1645, May 2014.
- [28] mmMagic Deliverable D1.1, "Use case characterization, KPIs and preferred suitable frequency ranges for future 5G systems between 6 GHz and 100 GHz," Nov. 2015, available at: <https://5g-mmmagic.eu/results/>.
- [29] Ericsson AB, "Delivering high-capacity and cost-efficient backhaul for broadband networks today and in the future," Sept. 2015, available at: <http://www.ericsson.com/res/docs/2015/microwave-2020-report.pdf>.
- [30] European Commission 5G project, "Mm-wave based mobile radio access network for 5G integrated communications," <https://5g-ppp.eu/mmmagic/>.
- [31] H. Xu, T. S. Rappaport, R. J. Boyle, and J. H. Schaffner, "Measurements and models for 38-GHz point-to-multipoint radiowave propagation," *IEEE J. Sel. Areas Commun.*, vol. 18, no. 3, pp. 310–321, March 2000.
- [32] D. Beauvarlet and K. L. Virga, "Measured characteristics of 30-GHz indoor propagation channels with low-profile directional antennas," *IEEE Antennas Wireless Propag. Lett.*, vol. 1, no. 1, pp. 87–90, 2002.
- [33] A. Annamalai, G. Deora, and C. Tellambura, "Analysis of generalized selection diversity systems in wireless channels," *IEEE Trans. Veh. Technol.*, vol. 55, no. 6, pp. 1765–1775, Nov. 2006.
- [34] E. Bjornemo, "Energy constrained wireless sensor networks: communication principles and sensing aspects," Ph.D. dissertation, Uppsala University, Uppsala, Sweden, 2009.
- [35] D. Persson, T. Eriksson, and E. G. Larsson, "Amplifier-aware multiple-input multiple-output power allocation," *IEEE Commun. Lett.*, vol. 17, no. 6, pp. 1112–1115, June 2013.
- [36] ———, "Amplifier-aware multiple-input single-output capacity," *IEEE Trans. Commun.*, vol. 62, no. 3, pp. 913–919, March 2014.
- [37] B. Makki, T. Svensson, T. Eriksson, and M. Nasiri-Kenari, "On the throughput and outage probability of multi-relay networks with imperfect power amplifiers," *IEEE Trans. Wireless Commun.*, vol. 14, no. 9, pp. 4994–5008, Sept. 2015.
- [38] G. Caire and D. Tuninetti, "The throughput of hybrid-ARQ protocols for the Gaussian collision channel," *IEEE Trans. Inf. Theory*, vol. 47, no. 5, pp. 1971–1988, July 2001.
- [39] B. Makki and T. Eriksson, "On the performance of MIMO-ARQ systems with channel state information at the receiver," *IEEE Trans. Commun.*, vol. 62, no. 5, pp. 1588–1603, May 2014.
- [40] H. E. Gamal, G. Caire, and M. O. Damen, "The MIMO ARQ channel: Diversity-multiplexing-delay tradeoff," *IEEE Trans. Inf. Theory*, vol. 52, no. 8, pp. 3601–3621, Aug. 2006.
- [41] D. Tuninetti, "On the benefits of partial channel state information for repetition protocols in block fading channels," *IEEE Trans. Inf. Theory*, vol. 57, no. 8, pp. 5036–5053, Aug. 2011.
- [42] S. M. Aghajanzadeh and M. Uysal, "Information theoretic analysis of hybrid-ARQ protocols in coherent free-space optical systems," *IEEE Trans. Commun.*, vol. 60, no. 5, pp. 1432–1442, May 2012.
- [43] Wolfram, "The wolfram functions site," [Online], Available: <http://functions.wolfram.com>, 2016.
- [44] I. S. Gradshteyn and I. M. Ryzhik, *Table of Integrals, Series, and Products*. 7th edition. Academic Press, San Diego, 2007.

- [45] F. Yilmaz and M.-S. Alouini, "Product of shifted exponential variates and outage capacity of multicarrier systems," in *Proc. European Wireless*, Alborg, Denmark, May 2009, pp. 282–286.
- [46] R. A. Horn and C. R. Johnson, *Matrix Analysis*. Cambridge University Press, 1985.